Bulgarian Chemical Communications, Volume 45, Special Edition A (pp. 88 – 93) 2013

Anodic oxidation mechanism of aluminum alloys in a sulfate-fluoride electrolyte

Ch.A. Girginov*, M.S. Bojinov

Department of Physical Chemistry, University of Chemical Technology and Metallurgy, 1756 Sofia, Bulgaria

Received February 28, 2013; Revised March 21, 2013

In recent years, fluoride containing electrolytes are used for the formation of porous structures on valve metals such as Ti, Nb, W, Ta and alloys thereof. The presence of fluoride ions allows the growth of nanoporous/nanotubular templates with well-defined structures. Very recently neutral sulfate-fluoride solutions have been successfully used to form nanoporous films on Al as well. As a continuation of this work, the present study reports on the initial stages of growth of porous anodic films on two Al alloys in fluoride-containing electrolytes by voltammetry and electrochemical impedance spectroscopy. A kinetic model based on the surface charge approach was employed to fit the impedance spectra and to estimate the main transport parameters of the oxide formation and dissolution process as depending on applied potential and alloy type.

Key words: aluminium alloy, sulfate-fluoride electrolyte, nanoporous alumina, electrochemical impedance spectroscopy, surface charge approach

INTRODUCTION

In recent years, there has been a growing interest towards the electrochemical formation of nanoporous and nanotubular structures on a number of valve metals, including Al and its alloys [1-9]. Nanoporous anodic films on aluminum and its alloys allow the incorporation of metallic or oxide nanoparticles within their pores, resulting in the production of new functional nanomaterials. These materials find increasing application as sensors, catalysts, electrodes for fuel cells and batteries with enhanced photo-catalytic and electro catalytic activity.

Neutral fluoride-containing electrolytes are widely used for the formation of porous structures on Ti, Nb, W, Ta, Zr, as well as on Al [10-13]. In that respect, the present paper aims at investigating the initial stages of nanoporous alumina formation in a neutral fluoride-containing electrolyte. First, results from electrochemical measurements (cyclic voltammetry, chronoamperometry and electro-chemical impedance spectroscopy) are reported and discussed in view of the parallel processes of alumina formation and dissolution of the substrate through the forming oxide. Second, the surface charge approach proposed earlier by some of us [14] is adapted to the aluminum/oxide/electrolyte system and by fitting EIS data to the transfer function of the model, the main transport parameters of the model are estimated as depending on applied potential and alloy type.

EXPERIMENTAL

The electrodes (4 cm^2) were cut from pure aluminum (99.999%) sheets and two aluminum alloys: 8006 (97.90% Al, 0.25% Si, 1.44% Fe, and 0.37% Mn) and 8011 (98.55% Al, 0.66% Si, 0.70% Fe, and 0.06% Mn). The specimens were then degreased and electro polished in a phosphoric-chromic acid electrolyte (210 cm^3 H_2O, 40 g CrO3, 450 g 85 % H_3PO_4, 150 g 96 % H_2SO_4) at 80°C and by constant anodic current density of 0.2 – 0.3 A cm^{-2} for ca. 3 min. Finally, they were rinsed with bi-distilled water and dried at 40°C in air. Prior to the experiments, the electrodes were brightened in an aqueous solution (1.8% CrO_3 and 7% H_3PO_4) at 75°C for 3 minutes and rinsed with bi-distilled water.

The electrochemical measurements were carried out at constant temperature (20±1 °C) in a three-electrode cell featuring a Pt-mesh counter electrode, situated symmetrically around the working electrode, and a Ag/AgCl/3M KCl reference electrode. An electrolyte with a composition of 0.5M $(NH_4)_2SO_4$ + 0.075M NH_4F, prepared from analytical grade chemicals and bi-distilled water, was employed. Electrochemical measurements were carried out with an Autolab PGSTAT 30 with a FRA2 module driven by GPES and FRA software (Eco Chemie, The Netherlands). Current density vs. time dependencies were registered by 1 h of polarization at each applied potential (-1.2 V to 5.0 V). After reaching a constant value of the current density at a given potential, electrochemical impedance spectra were measured in the frequency

* To whom all correspondence should be sent:
E-mail: christian.girginov@gmail.com

range (10 mHz to 10 kHz) with an amplitude of 10 mV of the superimposed AC signal (rms). Fitting of the impedance spectra to equivalent circuits has been performed using ZView software (Scribner).

RESULTS AND DISSCUSSION

Current vs. potential curves

The steady-state current-potential curves for the studied alloy types compared to pure Al (Fig. 1) suggest several process stages:

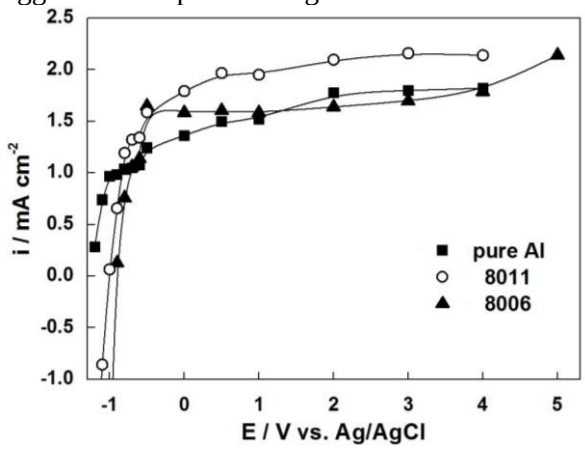

Fig. 1 Current vs. potential curves for pure Al and the two studied alloys in sulfate-fluoride electrolyte

i. Quasi-exponential increase of the current (-1.2/-0.9 V) due to dissolution of Al (and other alloying elements) superimposed to hydrogen evolution

ii. Much slower increase of the current (-1.0/0.0 V) that can be associated with barrier layer formation (passivation)

iii. At ca. 0-0.5 V, a current plateau is reached, indicating that chemical dissolution of the oxide is rate determining. At still higher potentials, there is some indication of current increase, especially for the 8006 alloy.

The obtained results for the three alloy types demonstrate that the current densities vs. potential dependences are qualitatively similar. At the most negative potentials, hydrogen evolution predominates over Al dissolution for both alloys, which can be due to preferential reduction of water on secondary Si, Fe and Mn-containing phases. On the other hand, the higher current density in the passive range registered for 8011 Al alloy was apparently due to the greater amount of the alloying element Si which is actively complexed by fluoride ions.

Impedance spectra

Impedance spectra have been recorded in the range of potentials -1.2 to 5.0 V. Typical spectra at several potentials as depending on the type of material are shown in Fig. 2-Fig.4.

The spectra consist of three time constants: high-frequency capacitive, intermediate -frequency pseudo-inductive and a further low frequency capacitive. These time constants can be interpreted as a first approximation by taking into account the migration of main current carriers (probably oxygen vacancies) and recombination of oppositely charged current carriers. The capacitive branch detected at lowest frequencies can be interpreted by a thickness modulation at a constant potential

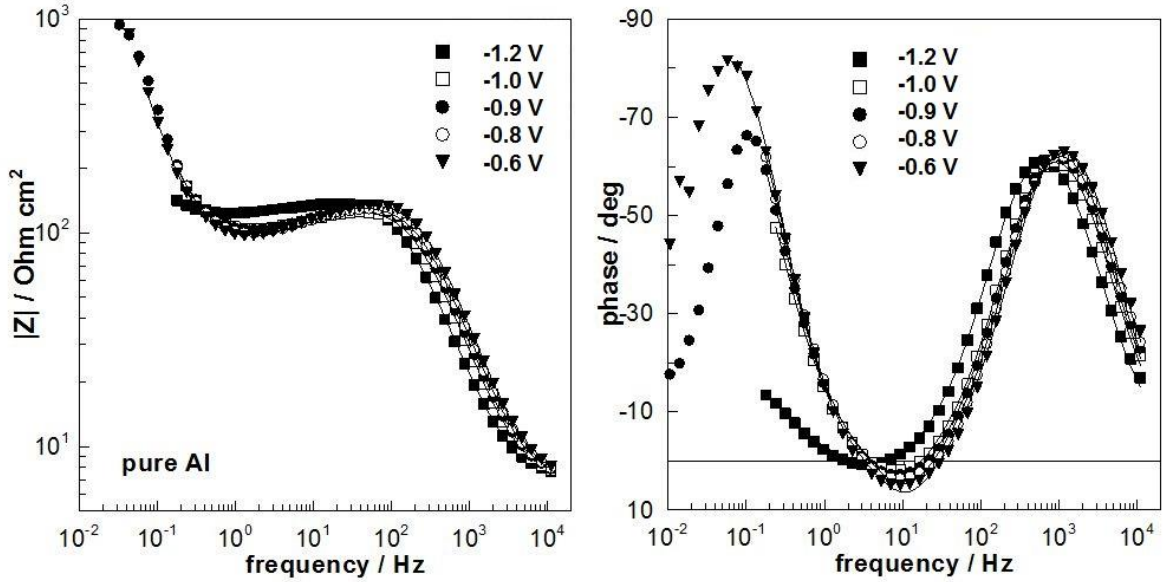

Fig. 2 Electrochemical impedance spectra of pure Al in the range of potentials -1.2 to -0.6 V. Left-impedance magnitude vs. frequency, right – phase angle vs. frequency. Points – experimental data, solid lines – best-fit calculation.

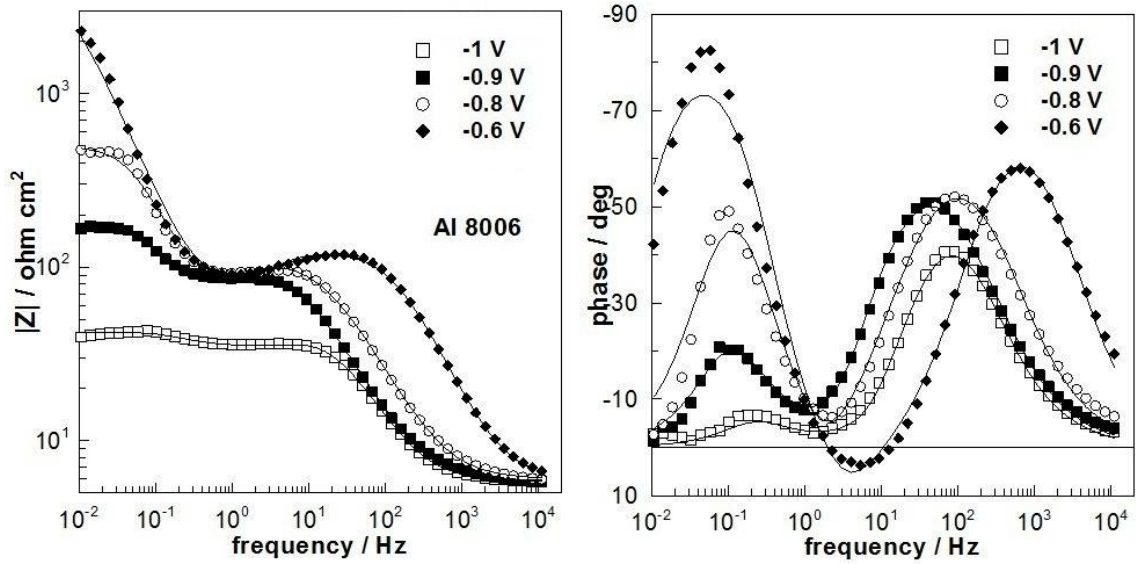

Fig. 3 Electrochemical impedance spectra of 8006 alloy in the range of potentials -1.2 to -0.6 V. Left-impedance magnitude vs. frequency, right – phase angle vs. frequency. Points – experimental data, solid lines – best-fit calculation.

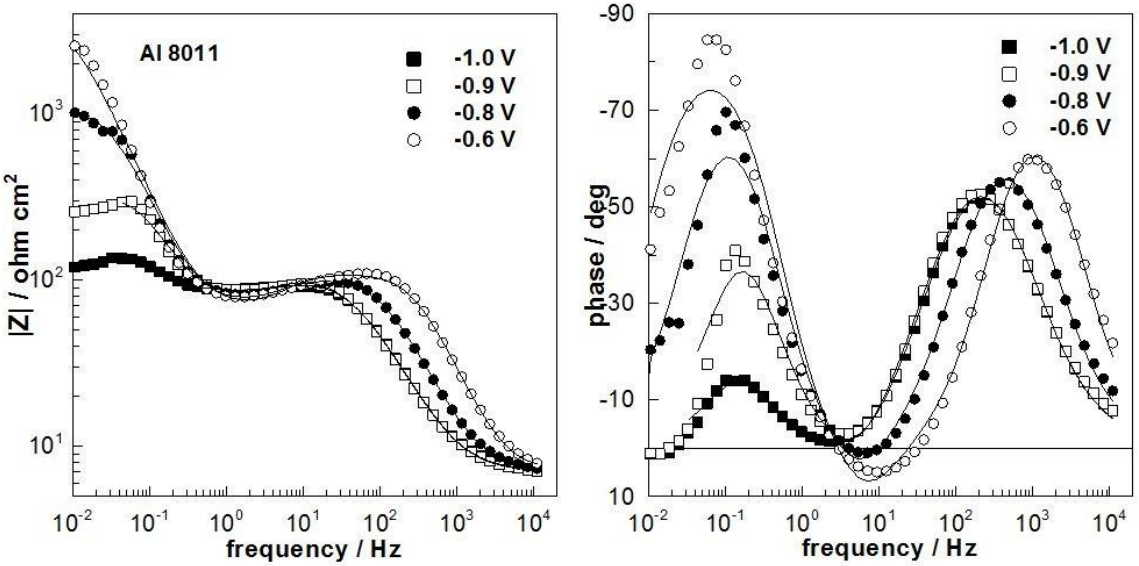

Fig. 4 Electrochemical impedance spectra of 8011 alloy in the range of potentials -1.2 to -0.6 V. Left-impedance magnitude vs. frequency, right – phase angle vs. frequency. Points – experimental data, solid lines – best-fit calculation.

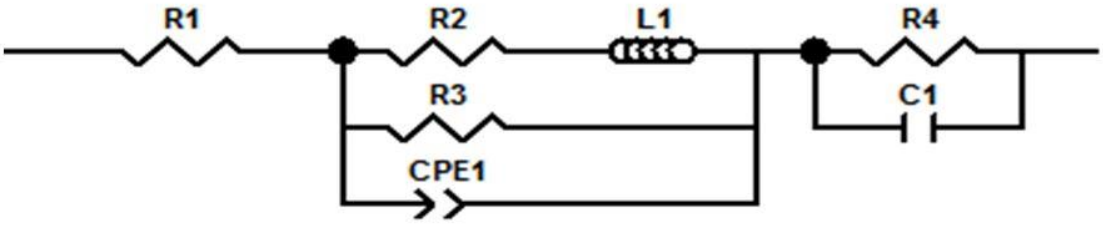

Fig. 5 Equivalent circuit according to the surface charge approach [14]. R_1 – electrolyte resistance, R_2 – surface charge resistance, L_1 – surface charge pseudo-inductance, R_3 – ion migration resistance, CPE_1 – oxide capacitance generalized in the form of a constant phase element, R_4 – charge transfer resistance at the film/solution interface, C_1 – faradaic and/or adsorption pseudo-capacitance.

due to the ac signal or by slow adsorption of some intermediate species of the overall reaction. Thus the obtained spectra can be compared with an appropriate equivalent circuit [14] (Fig. 5). Fits to this equivalent circuit are presented in Fig.2-4 with solid lines and illustrate the ability of this model to reproduce the data for all the studied materials. The parameters of the equivalent circuit for both alloys and pure aluminum are determined for all applied potentials.

At this stage of the investigation, main attention is paid to the parameters associated with film growth. According to the surface charge approach [14], the following dependences of the parameters on the applied potential (E) and current density (i) are predicted:

$$R_3\, i = \left(RT / 2Fa\boldsymbol{E}_{\mathbf{F}}\right)E$$

$$R_2\, i = \left[\left(1-\alpha\right)/\alpha\right]\left(RT / 2Fa\boldsymbol{E}_{\mathbf{F}}\right)E$$

$$L_1\, i^2 = \left[\left(1-\alpha\right)/\alpha\right]\left(RT / 2FaS\boldsymbol{E}_{\mathbf{F}}\right)E$$

where E is the applied potential, a is the half-jump distance (cm), EF - field strength in the oxide (V cm-1), α - part of the applied potential consumed at the oxide/solution interface as opposed to film bulk and S - capture cross-section for a point defect (cm2 C-1). In addition, for a quasi-dielectric oxide (i.e. a total depletion of the film with electronic charge carriers) the high-frequency film capacitance is given by

$$C_{\mathrm{b}} = \varepsilon\varepsilon_0\boldsymbol{E}_{\mathbf{F}} / \left(1-\alpha\right)E$$

The film capacitance was estimated from the CPE element in Fig.5 by using the formula proposed by Brug et al. [15].

The values of Cb, R_3i, R_2i and L_1i^2 as depending on the applied potential are presented in Fig. 6.

All the dependences in Fig. 6 are linear in the range of potentials -0.5 to 5.0 V, further supporting the validity of the model. At lower potentials, a more complex interplay between film growth and dissolution is observed for the alloys. From the obtained linear dependences, the main transport parameters of oxide growth are estimated and collected in Table 1 as depending on alloy composition.

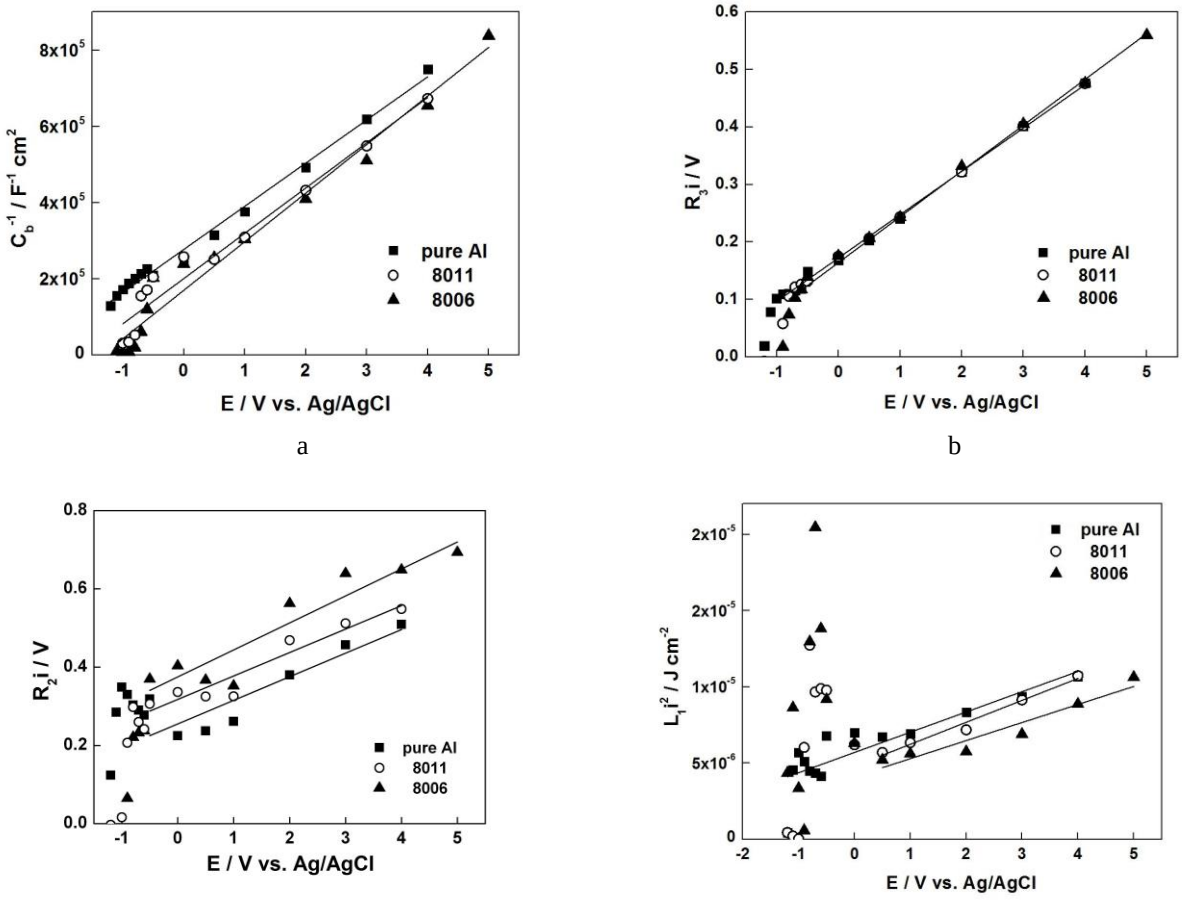

Fig. 6 Dependences of the equivalent circuit parameters associated with film growth and dissolution on applied potential

Table 1. Transport parameters estimated from the fitting of the impedance data to the model equations. A value of 8.9 was adopted for the dielectric constant of the oxide.

Material	α	E_F / MV cm^{-1}	(1-α) E_F^{-1} / nm V^{-1}	a / nm	S / cm^2 mC^{-1}
Pure Al	0.51	5.46	0.90	0.31	58.7
8006	0.44	5.91	0.94	0.27	53.1
8011	0.49	5.07	1.01	0.31	52.4

The values of the parameters are only slightly dependent on alloy composition and exhibit values in agreement with those recently estimated for the anodic oxides on Al in sulfuric acid-oxalic acid mixtures using fitting of EIS data by the surface charge approach [16]. In particular, the anodizing ratio is very close to that usually reported for sulfuric acid anodizing [17]. The main differences between the alloys and pure Al are in the parameter S characterizing to the formation of negative surface charge at the film/solution interface, which in turn is related to dissolution of the alloying elements. In order to correlate this to the properties of the oxide formed on the alloys, additional data on its composition and structure are needed. Such data are being produced and will be reported in the near future.

CONCLUSIONS

In the present work, an investigation of the initial stages of anodic alumina growth in neutral sulfate-fluoride electrolyte using voltammetry and electrochemical impedance spectroscopy is reported. The following conclusions can be drawn on the basis of the obtained results:

- Voltammetric results indicate that at the most negative potentials, hydrogen evolution predominates over Al dissolution for both alloys, which can be due to preferential reduction of water on secondary Si, Fe and Mn-containing phases. On the other hand, the higher current density in the passive range registered for 8011 Al alloy was apparently due to the greater amount of the alloying element Si which is actively complexed by fluoride ions.
- A kinetic model based on the surface charge approach employed to fit the impedance spectra and to evaluate the dependences of the main parameters of the oxide formation and dissolution on alloy type.
- Fitting of the impedance spectra to the equations of the surface charge approach adapted to the aluminum oxide growth demonstrated that the process of film thicknening is assisted by constant field strength, the anodizing ratio being within the range of values typical for porous anodic alumina.
- At lower potentials, a more complex interplay between film growth and dissolution is observed for the alloys. Additional data on the composition and structure of the surface film as depending on potential and alloy composition are needed in order to establish a quantitative correlation between film nature, its electric and electronic properties.

Acknowledgement: *The financial support of the National Science Fund, Contract No. DDVU 02/103-2010 "Nanoporous anodic oxides as a new generation of optically active and catalytic materials (NOXOAC)" is gratefully acknowledged.*

REFERENCES

1. D. Gong, C.A. Grimes, O.K. Varghese, Z. Chen, E.C. Dickey, *J. Mater. Res*., **16,** 3334(2001).
2. M.S. Gudiksen, L.J. Lauhon, J.F. Wang, D.C. Smith, C.M. Lieber, *Nature,* **415,** 617 (2002).
3. K. Lee, U. Goesele, K. Nielsch, *Nature Mater.,* **5,** 741 (2006).
4. J. Macak, K. Sirotna, P. Schmuki, *Electrochim. Acta,* **50,** 3679 (2005).
5. J. Macak, H. Tsuchiya, P. Schmuki, *Angewandte Chemie,* **44,** 2100 (2005).
6. Q. Cai, M. Paulose, O.K. Varghese, C.A. Grimes, *J. Mater. Res.,* **20,** 230 (2005).
7. L. V. Taveira, J. M. Macák, H. Tsuchiya, L. F. P. Dick, P. Schmuki, *J. Electrochem. Soc*. **152** (2005) B405.
8. I. Sieber, P. Schmuki, *J. Electrochem. Soc*. **152,** C639 (2005).
9. A. Ghicov, P. Schmuki, *Chem. Commun*., 2791 (2009).
10. H. Tsuchiya, S. Berger, J. M. Macak, A. G. Munoz, P. Schmuki, *Electrochem. Commun*,. **9,** 545 (2007).
11. C. Girginov, M. Bojinov, *Bulg. Chem. Comm.,* **42,** 312 (2010).
12. C. Girginov, M. Bojinov, In *Nanoscience and Nanotechnology 11*, E. Balabanova, I. Dragieva, Eds., Heron Press, 2011, 93-96.
13. E. Clark, Y. X. Gan, L. Su, *Nanoscience and Nanotechnology Letters,* **4,** 61 (2012).
14. M.Bojinov, *Electrochim. Acta,* **42,** 3489 (1997).
15. G. J. Brug, A.L.G. Van Den Eeden, M. Sluyters-Rehbach, J.H. Sluyters, *J. Electroanal. Chem.,* **176,** 275 (1984).
16. R. Giovanardi, C. Fontanesi, W.Dallabarba, *Electrochim. Acta,* **56**, 3158 (2011).
17. J. W. Diggle, T.C. Downie, C. W. Goulding, *Chem. Rev.,* **69**, 365 (1969).

МЕХАНИЗЪМ НА АНОДНО ОКИСЛЕНИЕ НА АЛУМИНИЕВИ СПЛАВИ В СУЛФАТНО-ФЛУОРИДЕН ЕЛЕКТРОЛИТ

К. А. Гиргинов*, М. С. Божинов

Катедра Физикохимия, Химикотехнологичен и металургичен университет, 1756 София, България

Постъпила на 28 февруари, 2013 г.; Коригирана на 21 март, 2012 г.

(Резюме)

През последните години, флуорид-съдържащи електролити се използват за формиране на порести структури върху вентилни метали като Ti, Nb, W, Ta и техни сплави. Наличието на флуоридни йони позволява растежа на нанопорести / нанотубуларни матрици с добре дефинирани структури. Съвсем наскоро са били успешно използвани неутрални сулфатнофлуоридни електролити за формиране на нанопорести филми и върху алуминий. Настоящото изследване е посветено на началните етапи на растеж на порести анодни филми върху две алуминиеви сплави в тези електролити чрез волтамметрия и електрохимична импедансна спектроскопия. Приложен е кинетичен модел, основан на подхода на повърхностните товари, за интерпретация на получените импедансни спектри. Оценени са основните транспортни параметри при процесите на формиране и разтваряне на оксида в зависимост от приложения потенциал и вида на сплавта.